

et al. (1991) in this respect is that for the locked wave, the assumption of a single wave group has been used. However, after progressing over an uneven bottom part, usually the wave group is split in two or more groups with their own velocity. At the inflow boundary, one can make sure that a single wave group is entering the computational domain. This restriction can also be rephrased in the following way: the coupling between the wave envelope and the long wave should be weak or the coupling term $\mathcal{G}\bar{\phi}A$ should be weak.

From the computed results, the mean free-surface elevation $\bar{\zeta}$ follows from Eq. (182a).

The determination of the free and bound components can be performed only for a horizontal bottom. Because both $\partial\bar{\phi}/\partial t$ and $\partial\bar{\phi}/\partial x$ are available from the numerical computation, we also have,

$$\frac{\partial\bar{\phi}}{\partial t} = \frac{\partial\bar{\phi}_\ell^+}{\partial t} + \frac{\partial\bar{\phi}_f^+}{\partial t} + \frac{\partial\bar{\phi}_f^-}{\partial t} \quad \text{and} \quad \frac{\partial\bar{\phi}}{\partial x} = \frac{\partial\bar{\phi}_\ell^+}{\partial x} + \frac{\partial\bar{\phi}_f^+}{\partial x} + \frac{\partial\bar{\phi}_f^-}{\partial x}. \quad (195)$$

The sets (193) and (195) yield five equations for six unknowns. Together with Eq. (186), the system is closed and can be solved. The splitting in free and bound wave components is thus achieved for a horizontal bottom only. This procedure is usually also used for uneven bottom with the understanding that the procedure then is not very accurate but with the hope of sufficient accuracy. However, this is still to be proven. The solution of these six equations leads to:

$$\partial_x\bar{\phi}_f^+ = \partial_x\bar{\phi} - C_1 - C|A|^2, \quad \partial_x\bar{\phi}_f^- = C_1, \quad \partial_x\bar{\phi}_\ell^+ = C|A|^2, \quad (196a)$$

with

$$C = \frac{1}{c_g^2 - gh} \left[\frac{g^2k}{2\omega} + c_g \left(\frac{\omega}{2 \sinh kh} \right)^2 \right], \quad (196b)$$

and

$$C_1 = \frac{1}{2c} [\partial_t\bar{\phi} + c\partial_x\bar{\phi} - (c - c_g)C|A|^2], \quad (196c)$$

and $c = \sqrt{gh}$. The solutions for $\partial_t\bar{\phi}_f^+$, $\partial_t\bar{\phi}_f^-$ and $\partial_t\bar{\phi}_\ell^+$ follow immediately from Eqs. (193). An example is given in Dingemans *et al.* (1991).

8. Observations of Wave Modulations

8.1. Theoretical aspects of modulational instability

Basic ideas of Benjamin–Feir instability mechanism have been presented in the introductory section 2. The first mathematical treatment of instability of water

waves was presented by Benjamin and Feir (1967). In an alternative approach, instability of water waves can also be analysed on the basis of modulation equations. While instability analysis based on the classical NLS equation leads to identical results as derived by Benjamin and Feir, use of higher-order modulation equation leads to improved results. We skip the details of the stability analysis based on the NLS equation which may be found in several books (e.g., Dingemans, 1997, p. 931ⁱ) and present some results for one-dimensional wave propagation. In short, proceeding with the equation,

$$i \frac{\partial A}{\partial \tau} + \lambda_1 \frac{\partial^2 A}{\partial \xi^2} - \nu_1 |A|^2 A = 0, \quad (197)$$

where the coefficients λ_1 and ν_1 are defined according to the Davey–Stewartson equation (section 3), one may seek solution to the amplitude envelope $A(\xi, \tau)$ in the form,

$$A(\xi, \tau) = a(\xi, \tau) \exp[i\chi(\xi, \tau)]; \quad a = a_0 + b(\xi, \tau). \quad (198)$$

In the assumed form, a_0 is the amplitude of the uniform Stokes solution and b is the perturbation, the nature of which needs to be investigated. The main conclusions are that for a perturbation of the form $b(\xi, \tau) = \hat{b} \exp[i(\kappa\xi - \Omega t)]$,

- (1) $\Omega^2 = \lambda_1 \kappa^2 (\lambda_1 \kappa^2 + 2\nu_1 a_0^2)$.
- (2) Instability occurs for $\Omega^2 < 0$, i.e., $\lambda_1^2 \kappa^2 + 2\lambda_1 \nu_1 a_0^2 < 0$. For real solutions of κ , this condition is met only if $\lambda_1 \nu_1 < 0$, equivalently, $\nu_1 > 0$ because $\lambda_1 < 0$ always. This is equivalent to the condition that $kh > 1.363$.
- (3) With $kh > 1.363$, the waves are unstable to a perturbation κ such that:

$$\frac{1}{2} \kappa^2 < -\frac{\nu_1}{\lambda_1} a_0^2;$$

in deep water ($kh \rightarrow \infty$), this condition translates to $(\kappa/k) < 2\sqrt{2}ka_0$.

- (4) Under the condition of instability, the growth rate $\text{Im}(\Omega)$ is:

$$\text{Im}(\Omega) = \kappa \left(|\lambda_1 \nu_1| a_0^2 - \frac{1}{2} \lambda_1^2 \kappa^2 \right)^{1/2}. \quad (199)$$

As may be seen from Eq. (199), the growth rate has a maximum and is therefore responsible for selective magnification of perturbation modes. For deep water

ⁱAn error has crept into the analysis presented in that section. The origin of the error is the coefficient of the term $a_{\tau\tau}$ in Eq. (8.227a) on p. 931 which should have been 1/2.

waves, perturbations $\kappa/k < 2\sqrt{2}ka_0$ are unstable and the maximum growth rate occurs for $\kappa/k = 2ka_0$ at which the growth rate Ω_m is $\omega(ka_0)^2/2$.

Exact analysis of Longuet-Higgins (1978) for deep water reveals marked differences from the preceding results based on the NLS equation. This difference is reduced by using higher-order modulation equation. An illustrative example of this is provided by Dysthe (1979). From Dysthe's analysis, valid only for deep water, the perturbation modes for instability and the maximum growth rate are:

$$\frac{\kappa}{k} \leq 2\sqrt{2}ka_0\sqrt{1 - \left|\frac{\kappa}{k}\right|}, \tag{200a}$$

$$\text{Im}(\Omega)|_{\text{max}} = \frac{\omega}{2}(ka_0)^2[1 - 2(ka_0)]. \tag{200b}$$

The normalised maximum growth rates $(\text{Im}(\Omega)|_{\text{max}}/\omega)$ as predicted by the NLS and Dysthe's theory are shown for deep water case in Fig. 5.

The presence of a varying current makes the medium inhomogeneous for waves. Equivalently, this is reflected in the coefficients of the Schrödinger equation having both temporal and spatial variation. While the essence of the stability analysis remains the same as before, a general analysis of the side-band instability due to the inhomogeneity introduced by a current becomes difficult.

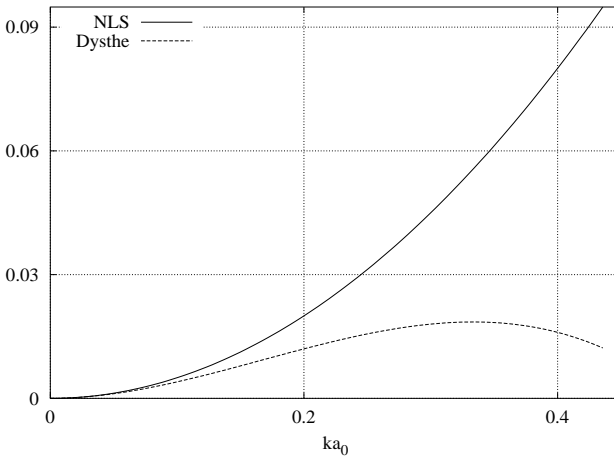


Fig. 5. The normalised maximum growth rate $(\text{Im}(\Omega)|_{\text{max}}/\omega)$ as a function of steepness ka_0 from NLS and Dysthe's theory.

Here, we discuss some results, due to Gerber (1987), which are valid only for deep-water. For waves with a constant dominant wave vector $\mathbf{k} = (k, 0)^T$, the current-modified Schrödinger equation used in the analysis is:

$$i \left[\frac{\partial A}{\partial t} + (c_g + U) \frac{\partial A}{\partial x} + \left(\frac{1}{2} \frac{dc_g}{dx} + \frac{3}{4} \frac{dU}{dx} \right) A \right] - \frac{1}{8} \frac{\omega_r}{k^2} \frac{\partial^2 A}{\partial x^2} + \frac{1}{4} \frac{\omega_r}{k^2} \frac{\partial^2 A}{\partial y^2} - \frac{1}{2} \omega_r k^2 |A|^2 A = 0, \quad (201)$$

where U is a slowly-varying current and ω_r is the linear relative frequency equal to \sqrt{gk} . To discuss the effect of an ambient current collinear to the wave direction, we consider the one-dimensional version of Eq. (201) in which case, the derivatives with respect to y are omitted.

Unlike in case of waves alone, the Stokes solution in the presence of a varying current is no longer of uniform amplitude. The solution to Stokes amplitude $a_0(x)$ is given by:

$$a_0(x) = \tilde{a}_0 \exp \left[- \int_{x_0}^x dx \left(\frac{\frac{1}{2} \frac{dc_{gr}}{dx} + \frac{3}{4} \frac{dU}{dx}}{c_{gr} + U} \right) \right], \quad (202)$$

where \tilde{a}_0 is the amplitude at $x = x_0$. The relationship between Ω and the perturbation mode κ is found to be,

$$\Omega^2 = \frac{\omega_r^2 \kappa^2}{8k^2} \left\{ \frac{\kappa^2}{8k^2} - k^2 \tilde{a}_0^2 \exp \left[- \int_{x_0}^x dx \left(\frac{\frac{dc_g}{dx} + \frac{3}{2} \frac{dU}{dx}}{c_g + U} \right) \right] \right\}. \quad (203)$$

Thus, instability occurs for,

$$0 < \frac{\kappa}{k} \leq 2\sqrt{2}k\tilde{a}_0 \exp \left[- \int_{x_0}^x dx \left(\frac{\frac{1}{2} \frac{dc_g}{dx} + \frac{3}{4} \frac{dU}{dx}}{c_g + U} \right) \right]. \quad (204)$$

Equation (204) is equivalent to the case of waves only if the current gradient is zero. Secondly, utilising Eq. (202), the stability condition

$$0 < \frac{\kappa}{k} \leq 2\sqrt{2}ka_0 \quad (205)$$

becomes identical to the Benjamin–Feir condition for waves in terms of the local steepness ka_0 . Thus, under the assumption that the group length scale is much smaller than the scale of current variation, the stability criterion remains

unchanged in terms of local wave steepness. The local steepness is of course modified by the variation of the current from its original value.

For the specific case of initial current being zero ($\tilde{U} = 0$), explicit use of the deep water relationship in Eq. (204) leads to:

$$0 < \frac{\kappa}{\tilde{\kappa}} \leq \frac{64\sqrt{2}\tilde{k}\tilde{a}_0}{[1 + 4\frac{U}{\tilde{c}}]^{\frac{1}{4}}(1 + [1 + 4\frac{U}{\tilde{c}}]^{\frac{1}{2}})^5}, \tag{206}$$

where all the variables with the superscript “tilde” denote their initial values. It is evident from Eq. (206) that an opposing current ($U/\tilde{c} < 0$) increases the region of instability whereas a following current has the reverse action. It follows further from Eq. (203) that the maximum growth rate occurs for,

$$\frac{\kappa}{k} = 2(k\tilde{a}_0) \exp \left[- \int_{x_0}^x dx \left(\frac{\frac{1}{2} \frac{dc_g}{dx} + \frac{3}{4} \frac{dU}{dx}}{c_g + U} \right) \right], \tag{207}$$

at which the growth rate Ω is given by:

$$\frac{\text{Im}(\Omega)}{\omega_r} \Big|_{\text{max}} = \frac{1}{2} (k\tilde{a}_0)^2 \exp \left[- \int_{x_0}^x dx \left(\frac{\frac{dc_g}{dx} + \frac{3}{2} \frac{dU}{dx}}{c_g + U} \right) \right]. \tag{208}$$

8.2. Laboratory observations

Following the observations of instability of deep water waves by Feir as reported in Benjamin (1967), several experimental investigations of the modulational behaviour have been undertaken to date. Almost all of the reported experiments over this pertain to deep water waves (see Table 1 in Tulin and Waseda, 1999) except perhaps a singular case (Shemer *et al.*, 1998). More experiments over finite depth may therefore be suggested to cover a broader range.

Limited length of the wave flumes and energy damping due to side-wall boundary layers are two factors which make interpretations of experimental results difficult. The other factor is the background noise or specific seeding of the input signal in the experiments. Experiments without seeding show that background noise is enough to lead to modulational instability. One of the sources of the background noise in the experiments is the transient front (Melville, 1982; Tulin and Waseda, 1999). Seeded experiments on the other hand make it easier to study growth in a controlled way with systematic variation of the amplitudes and frequencies of the disturbance modes. Modulation

and consequent increase in local steepness may lead to breaking depending on the initial wave steepness and disturbance parameters. We describe first the initial stage of modulation and demodulation for nonbreaking waves followed by modulation leading to breaking.

8.3. Deep-water modulation: initial stage and demodulation

A pioneering set of experiments in this regard is due to Yuen and Lake (1975) and Lake *et al.* (1977). Their experiments were carried out in a $0.9 \times 0.9 \times 12$ m tank. By using modulated input signals of prescribed side-bands, they were able to record measurable growth of the side-band amplitude along the length of the tank. For the purpose of laboratory experiments, spatial growth rate is more relevant than the temporal growth rate for which theoretical expressions have been presented in the preceding section. The equivalent spatial growth rate $\Omega^{(x)}$ of the side-band amplitude based on the linear stability analysis of Benjamin and Feir (1967) is given by:

$$\Omega^{(x)} = \Delta[2(ka_0)^2 - \Delta^2]^{\frac{1}{2}} k, \quad \delta = \frac{\Delta\omega}{\omega}. \quad (209)$$

Their measurements supported both the theoretical prediction (209) for the growth rate $\Omega^{(x)} = (d(\log S)/dx)$ (S being the side-band amplitude) and the earlier observations of Benjamin (1967). They observed, however, that the wave steepness measured near (but further away for evanescent modes) the wavemaker needs to be corrected before being used as the initial steepness of the carrier waves in the theoretical expression. It was construed (Lake and Yuen, 1977) that this correction was necessary to account for the apparent nonlinearity of waves, generated by a sinusoidally moving wavemaker, being smaller than the theoretical Stokes waves (with its bound superharmonics). From analysis of data of the side-band width Δ of the most unstable mode and the measured steepness, this correction was specified to be $(ka)_0 = 0.78(ka)_{\text{measured}}$. Later work (Longuet-Higgins, 1978) has shown that the analysis of Benjamin and Feir shows significant deviation from the exact values (potential flow) for $(ka)_0 > 0.1$. Thus, while the difference between Stokes waves and that generated by a sinusoidal wavemaker is a fact, the mismatch between the measured growth rate and that from Eq. (209) is also likely due to the small steepness limitation of the latter.

The exposition in Lake *et al.* (1977) went beyond the initial growth of instability. They gave evidence of demodulation, i.e., the waves tend to return

to their initial state existing before modulation. This observation that modulational instability does not necessarily lead to a disintegration of water waves renewed support to the recurrence of modulation exhibited by the NLS equation. However, there remained many questions hidden behind this evidence of near-recurrence and their data did not cover sufficient ground to clarify them. Many of the issues involved have been re-examined in the recent experiment by Tulin and Waseda (1999).

One of the cases investigated by Tulin and Waseda (1999) in a wave tank of $4.2 \times 2.1 \times 50$ m, corresponds to an initial steepness of 0.1 and a “seeded” modulation of $\delta\omega/\omega = 0.0894$. No breaking was observed and the length of the tank allowed the completion of one modulation cycle. This case is perhaps the best evidence of recurrence among reported laboratory studies. At the peak of the modulation near 25 m from the wavemaker, the amplitude at the carrier frequency had nearly vanished. Beyond this peak modulation, however, the waves evolved back nearly to the original three modes (carrier, upper and lower side-bands) before the end of the tank. This is a strong corroboration of the near recurrence referred to by Lake *et al.* (1977). As described later, for values of steepness and modulation band within a certain range, waves break during modulation. The long-term behaviour in those cases is markedly different than the near-recurrence of the wave modulation.

In the aforementioned recurrence of nonbreaking modulation, we have used the qualifier “near” indicating that the wave system does not exactly reset back to the initial three waves at the end of the modulation. One key difference is that the evolved spectrum shows a noticeable (on a log-linear scale) discretised high-frequency energy spread. Although the energy content of the spread is low, this feature may be responsible for the deviation from a perfect recurrence. Secondly, while Lake *et al.* (1977) found that the carrier waves experience a down-shift of the frequency, this down-shift was absent in Tulin and Waseda (1999) in the absence of breaking. This feature, if true, is another deviation from a perfect recurrence. In spite of these deviations being small, they are important in the sense that the tank length has limited such studies to a maximum of one modulational scale. Multi-cycle behaviour of these deviations for nonbreaking waves remains an interesting study.

In summary, it is important to recognise that side-band instability does not lead to breaking for waves of all steepness and all modulations. A rough guide to determine the region of breaking on the parameter space of $\varepsilon = (ka)_0$ and $\delta\omega/\omega$ is given by a diagram presented by Tulin and Waseda (1999) (their Fig. 17, p. 220). This diagram is based on experiments and fully nonlinear

computations over a range of ε and $\delta\omega/\omega$. Roughly, waves of initial steepness $(ka)_0$ smaller than 0.1 seem to be stable to undergo a modulation cycle without breaking. For larger steepness, the region of breaking is centered around the locus of maximum growth rate; i.e., $\Delta\omega/\omega \approx \sqrt{ka_0}$.

8.4. Deep-water modulation: modulation leading to breaking

For waves of initial steepness greater than 0.1 and modulational disturbances within a certain band, breaking occurs during evolution. For a systematic exposure on the observation of modulational behaviour during and after breaking, we turn mostly to the studies due to Melville (1982, 1983) and Tulin and Waseda (1999). Important contributions to this field have also been put forward by Ramamonjarisoa and Mollo-Christensen (1979) and Su and Green (1985).

Increase in local steepness during evolution leads to breaking. In the pre-breaking stage, the measured growth rate agrees well with the theory. The local steepness, expressed by^j $kH_m/2$, seems to lie in a range from 0.25 to 0.4. This value is lower than the theoretical value of 0.44 for maximum steepness of stable waves. One immediate consequence of wave-breaking is the loss of near-recurrence described in the previous section. Secondly, the energy distribution over the wave components during and after breaking is drastically modified. Aside from the energy loss due to breaking, a significant difference between modulation with breaking and without lies in the relative growth of the side-bands. This point is best illustrated in Fig. 6 (reproduction of Fig. 18 of Tulin and Waseda, 1999).

The amplitude of the lower side-band remains high after breaking while for cases of no-breaking the amplitude subsides significantly almost to its original state. In contrast, the upper side-band drops back from its peak towards its pre-growth value. Although the carrier wave recovers somewhat it stays lower than its initial value. Thus, two processes seem to be taking place: discriminatory energy loss from the carrier and upper side-band modes, and an irreversible energy transfer to the lower side-band. The latter conclusion is more difficult to justify due to the length limitation of the wave tanks in the two experiments (Melville, 1982; Tulin and Waseda, 1999). The end result is that the lower side-band remains most energetic after peak modulation and breaking resulting in a permanent down-shift of the spectral peak within the length of the tank.

^jIt is not perfectly clear whether k is the wave number of the carrier wave or the one of the modulated wave. The issue seems not to be very important since a range is defined.

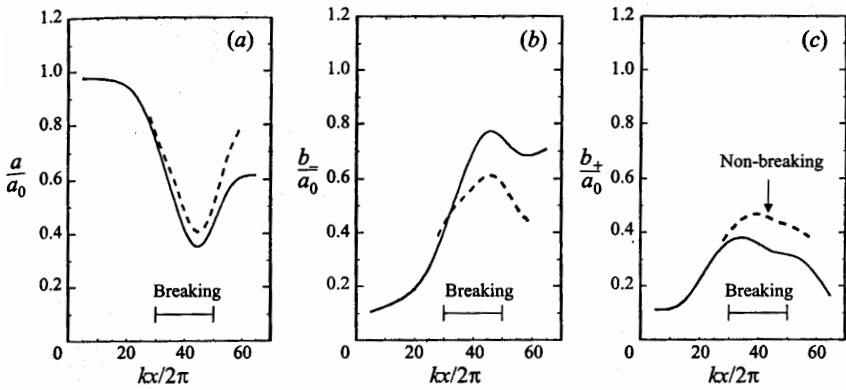


Fig. 6. Spatial modulation of carrier, sub and super side-band modes with and without breaking. Reproduced from Tulin and Waseda (1999) (Fig. 18, p. 221).

8.5. Spectral evolution

In the two preceding sections, evolution of only the side-bands and carrier waves have been discussed. Although an important part of the evolution process, behaviour of the side-band modes alone does not give the complete picture of the spectral transformation. Occurrence of discretised high-frequency spread of energy (seen clearly in log-linear plots) is another feature of importance with respect to the long-term evolution of the wave field. Melville (1982) was the first to draw attention to this aspect from his experimental results. He noted that aside from the spikes at the side-band frequencies, spikes appear at other frequencies. These spikes are first prominent at the subharmonic interaction frequency of $\Delta\omega$ and superharmonic modes $n\omega_0$ with n as an integer. With evolution downstream from the wavemaker, prominent spikes become more numerous in the discrete spectrum appearing for example at frequencies $\omega_0 + 2\Delta\omega$, $n(\omega_0 \pm \Delta\omega)$. At locations near and after breaking, there seems to be a trend towards a broad-band continuous spectrum around the primary frequency ω_0 . The initial steepness of waves used in Melville's experiments was 0.232 and 0.292 respectively. Tulin and Waseda (1999) observed that the generation of a continuous spectrum depended not only on the steepness but also on the bandwidth of the disturbance. From the known experimental cases, it does not seem feasible to conclusively specify the conditions which lead to a continuous spectrum. The results only show that under certain conditions, wave-breaking

during modulation is also associated with a scattering of energy from discrete spikes to a continuous spectrum apart from the energy dissipation.

8.6. Comparison between theory and experiment

Numerical investigations have been presented by several authors based on several forms of nonlinear equations. However, comparisons between experimental measurements and numerical solutions are somewhat less exhaustive and should be extended. The cubic NLS equation is the basic theoretical model for studying nonlinear modulation. Side-band instability which is a special class of nonlinear modulation is admitted by this theory. Both the unstable modes and the initial growth rate may also be extracted from this theory. More importantly, the theory predicts recurrence of modulation, a phenomenon which is clearly beyond the linear instability analysis. As mentioned in the previous section, for waves of initial steepness less than 0.1, laboratory observations show near recurrence. However, in spite of this success of the NLS equation in reproducing the broad features of the growth of side-band modes, peak modulation and subsequent demodulation and several other features remain unanswered attracting renewed attention for more advanced analysis.

In an inter-comparison study, Landrini *et al.* (1998) have compared the evolution behaviour predicted by NLS, mNLS, Zakharov's equation, Krasitskii's equation and the fully nonlinear potential flow computations. In consistence with the theoretical expectation, the computed results from an approximate equation system became closer to that from the fully nonlinear potential flow computation with increasing order of approximation. Fully nonlinear potential flow computations have been found to reproduce the experimental measurement of wave modulation up to the point of breaking (Tulin and Waseda, 1999). From whatever limited number of cases, fully nonlinear computations have been carried out seem to predict the breaking at the right location. Among the approximate nonlinear equations, NLS which is the simplest equation capable of modelling modulation does not reproduce any asymmetry. Comparisons by Shemer *et al.* (2000) between numerical computations and experimental observation show that asymmetry during the evolution of a group may be satisfactorily produced by mNLS and Zakharov's equation, the latter doing better. In an subsequent work, Shemer *et al.* (2001) have shown in a more elaborate way that the Zakharov equation could be used for an accurate description of the modulation and the skewed shape of the amplitude envelope of a wave field (non-breaking) during its evolution along a tank.

A major source of difficulty is the role of dissipation. Dissipation arises from the wall layer of the experimental flume and due to naturally occurring processes of surface wave-breaking. Many of laboratory and field observations are inseparably influenced by such dissipative mechanisms. Analysis of experimental measurements (Melville, 1982, 1983; Tulin and Waseda, 1999) indicate that energy transfer between wave components in the incipient stage of (and during) breaking happens rather rapidly in a complex way. Further understanding of this process is necessary to be able to enter the next stage of modelling in which post-breaking modulation may be calculated.

9. Summary

Wave transformation in the field involves wide-ranging processes including interactions among components and with varying depth and current. Modulation equations present a simpler framework with which both analytical and numerical insight and quantification of the processes may be achieved. An essential assumption in the derivation of the modulation equations is that length scale of variation of the amplitude envelope is much longer than that of the carrier waves. Thus, validity of such equations become limited when the wave properties (amplitude envelope, wave number) exhibit fast variation. With an ambient current, the current is assumed to be of large-scale compared to the waves. We also like to draw attention to the fact that 1D coherent wave groups (soliton-type solutions) are likely to become unstable in two dimensions. This is due to the instability of groups to oblique perturbations (e.g., Ablowitz and Segur, 1979). Because of this, coherent wave groups are more readily observed in wave flumes than in the field.

This review begins with some illustrative sections to guide uninitiated readers to the nonlinear processes in deep and intermediate water. Modulation equations involving cubic interactions have been presented for deep water followed by the more general cases of varying depth with or without an ambient current. Many theoretical descriptions deal with the classical case of deep water modulation. In engineering practices, the role of a finite and varying depth is important. The simplest form of equations on finite depth is the set of the so-called Davey–Stewartson equations [Eqs. (48)]. The cubic evolution equation on finite depth differs from the deep-water version in two ways. First, the coefficients of the equation depend on the depth. More importantly, the depth-averaged wave-induced current (long-wave) manifests itself in the amplitude modulation equation resulting in a coupling between the two. In 2D